Published in final edited form as:
J Phys Chem A. 2011 September 1; 115(34): 9536–9544. doi:10.1021/jp112324d.

Enzymatic Degradation of Multi-Walled Carbon Nanotubes

Yong Zhao, **Brett L. Allen**, and **Alexander Star**
Department of Chemistry, University of Pittsburgh, Pittsburgh, Pennsylvania 15260

Alexander Star: astar@pitt.edu

Abstract

Because of their unique properties, carbon nanotubes and in particular multi-walled carbon nanotubes (MWNTs) have been used for the development of advanced composite and catalyst materials. Despite their growing commercial applications and increased production, the potential environmental and toxicological impacts of MWNTs are not fully understood; however, many reports suggest that they may be toxic. Therefore, a need exists to develop protocols for effective and safe degradation of MWNTs. In this article, we investigated the effect of chemical functionalization of MWNTs on their enzymatic degradation with horseradish peroxidase (HRP) and hydrogen peroxide (H_2O_2). We investigated HRP/H_2O_2 degradation of purified, oxidized, and nitrogen-doped MWNTs and proposed a layer-by-layer degradation mechanism of nanotubes facilitated by side wall defects. These results provide a better understanding of the interaction between HRP and carbon nanotubes and suggest an eco-friendly way of mitigating the environmental impact of nanotubes.

After almost 20 years since their discovery,1 carbon nanotubes (CNTs) still spawn broad research interest in numerous disciplines and are a primary focus of nanoscience research. Their unique tubular graphitic structure and outstanding mechanical, electronic and chemical properties2–4 lead to a wide range of applications such as in composite materials,5,6 chemical sensing,7–9 and drug delivery.10,11 There are two main types of CNTs: single-walled carbon nanotubes (SWNTs) and multi-walled carbon nanotubes (MWNTs). MWNTs consist of several to dozens of concentric graphitic walls. Due to their low cost and large availability,12 MWNTs are advantageous over SWNTs for high volume applications such as composite materials. Their metallic nature also put forward the potential applications in fuel cells as electrode catalyst support.13 In addition, their multi-walled structure enhances their resistance to chemical treatment, which allows grafting of chemical functionalities at the surface of nanotubes while retaining their intrinsic mechanical and electrical properties.14 Acid oxidation is a common scheme of functionalizing MWNTs, which can introduce oxygen-containing defective sites within their outer graphitic walls,12,15 forming carboxylated MWNTs (o-MWNTs). Additionally, MWNTs can also be doped with heteroatoms such as nitrogen into the graphitic structures during the synthesis process,16 forming nitrogen-doped MWNTs (n-MWNTs) which were reported to have excellent catalytic activity in oxygen-reduction reaction (ORR).17,18 The promising applications of

Correspondence to: Alexander Star, astar@pitt.edu.

Supporting Information Available. The experimental procedures of Boehm's Titration, AFM, TGA and Amplex Red assay; TGA and EDS elemental analysis (Figure S1); histogram of surface acidic group loading on MWNTs (Figure S2); TGA curves for p-MWNTs, o-MWNTs (5hr) and o-MWNTs (8hr) in N_2 atmosphere (Figure S3); FTIR spectra for pretreated and carboxylated MWNTs (Figure S4); TEM images of MWNTs after degradation for 80 days (Figure S5); TEM and AFM images of carbonaceous flakes formed after degradation (Figure S6); Amplex Red assay for enzymatic activity (Figure S7); optical microscope images for Raman samples (Figure S8); high-resolution TEM images of o-MWNTs (8hr) and p-MWNTs before enzymatic degradation (Figure S9); TGA of n-MWNTs and TEM image of the control sample at Day 80 (Figure S10). This material is available free of charge via the Internet at http://pubs.acs.org.

MWNTs and their low cost of synthesis have spurred a global production about 40 times higher than SWNTs,19 which highly stressed the importance of investigating the enzymatic degradation of MWNTs as their potential disposal in the environment increases.

In addition to the potential environmental impact, there are reports that carbon nanomaterials may possess cytotoxicity, and pathogenicity.20–23 By functionalizing CNTs with various bioconjugates such as DNA,24 peptides25 or phospholipid components,26 the biocompatibility of carbon nanotubes is largely increased; still, CNTs remain resistant to physiological or environmental degradation under mild conditions in the long term, even after such functionalization.20,27 We have recently demonstrated that carboxylated SWNTs can be enzymatically degraded in the presence of low concentrations of H_2O_2 and peroxidases, such as horseradish peroxidase (HRP)28,29 and human myeloperoxidase (hMPO).30 As a result of their multi-walled morphology, MWNTs are considered more difficult to be degraded than SWNTs by enzymatic catalysis, which was shown in a recently published work.31 However, the detailed mechanism of MWNTs' enzymatic degradation is still ambiguous. In this study, we explored the enzymatic degradation of o-MWNTs with different degrees of carboxylation and n-MWNTs. A variety of characterization methods were implemented to monitor possible degradation including dynamic light scattering (DLS), transmission electron microscopy (TEM), Raman spectroscopy, and gas chromatography–mass spectrometry (GC-MS). For up to 80 days of degradation with daily additions of H_2O_2, o-MWNTs appeared to decrease in both diameter and length, although a complete disappearance of o-MWNTs was not observed. In contrast, when incubated under the same HRP/H_2O_2 conditions, n-MWNTs showed a complete degradation behavior within 80 days. In essence, these findings suggest that the presence of defects in MWNT sidewalls play a critical role in the enzymatic degradation process.

Experimental Section

Materials

MWNTs were received from Columbian Chemical Company (Marietta, GA). Lyophilized HRP type VI and 3% H_2O_2 were purchased from Sigma Aldrich. Amplex Red (10-acetyl-3,7-dihydroxyphenoxazine) was procured from Molecular Probes, Invitrogen.

Carboxylation of MWNTs

As-received MWNTs were pretreated by sonication in concentrated HNO_3 at room temperature for 4 hr in order to eliminate impurities such as amorphous carbon and metal catalysts. MWNTs were then filtered through a 0.22 μm Teflon membrane and washed with H_2O until a neutral pH was measured. Carboxylation of MWNTs was performed by sonicating approximately 10 mg of pretreated MWNTs in 5 mL of 3:1 H_2SO_4/HNO_3 mixture at 40 °C. (This solution is highly oxidizing. Caution must be taken when handling this system.) After 5 and 8 hours respectively, 2.5 mL of the suspension was taken out, diluted with 10 mL of double-distilled water, filtered through a 0.22 μm Teflon membrane, and washed with copious amounts of water until the pH was approximately 6 to 7. The pretreated MWNT samples are noted as "p-MWNT" and the 5 hr and 8 hr carboxylated samples are respectively noted as "o-MWNT (5hr)" and "o-MWNT (8hr)" herein and after.

Synthesis and purification of n-MWNTs

Nitrogen-doped MWNTs were synthesized using chemical vapor deposition (CVD) technique in a Lindberg/Blue tube furnace.16 The quartz substrate was placed in a three-foot long sealed quartz tube under 950 °C in the furnace. A liquid precursor containing 5.0 wt. % of MeCN, 1.25 wt. % of ferrocene, and 93.75 wt. % of EtOH was injected at a rate of 5 mL/

min in H_2 and Ar atmosphere. After 1 hr growth, the sample on the substrate was taken out and collected using a razor blade.

Purification of as-synthesized n-MWNTs was performed using the method adopted from Smalley et al.32 A sample of 4.4 mg as-synthesized n-MWNTs was suspended in a mixture of 2 mL HCl (1 M) and 2 mL H_2O_2 (30%) and stirred at 60 °C for 4.5 hr with the same amount of HCl and H_2O_2 supplemented every 1 hr. After filtration of the slurry and washing with copious amount of water, purified n-MWNT samples were collected and re-suspended in water.

Incubation with HRP and H_2O_2

Around 1 mg of p-MWNTs, o-MWNTs (5hr and 8hr), and n-MWNTs were transferred into four vials and sonicated in 4 mL of water for 1 hr to afford a stable suspension. HRP type VI aqueous solution (4 mL of 0.385 mg/mL) was then added into each vial followed by incubation for 24 hr. To start the degradation process, 8 mL of 800 μM H_2O_2 was added, and all vials were sealed with septum stoppers and wrapped with parafilm to keep them gastight. Additions of 250 μL of 800 μM H_2O_2 were performed on a daily basis to compensate for H_2O_2 consumption. All vials were placed on a rotary shaker with constant shaking (220 rpm) at room temperature in the dark to prevent photolysis of H_2O_2.33

Transmission Electron Microscopy (TEM)

TEM samples were prepared by centrifuging 250 μL the MWNT suspension at 3400 rpm for 2 hr. After removal of the supernatant, the precipitate was resuspended in 1 mL of EtOH through sonication, and around 10 μL of this suspension was dropped on a lacey carbon grid and dried in ambient conditions overnight for TEM imaging (FEI Morgagni, 80 keV, or JEOL 2100F, 200 keV). Alternatively, TEM sampling was done by directly drop-casting sample solution on to grids.

Raman Spectroscopy

Approximately 50 μL of sample suspension before and during degradation was drop-casted onto a quartz slide and dried under ambient conditions. Raman spectra were taken on a Renishaw inVia Raman microscope with an excitation wavelength of 633 nm. Spectra were scanned from 1000–1800 cm^{-1} for 5 times at 15 s exposure time. For each sample 5 Raman spectra from different sample spots were collected and averaged.

Gas Chromatography–Mass Spectrometry (GC-MS)

The CO_2 content in the headspace of the sample vials was measured with GC-MS. During the degradation process around 25 μL of headspace gases were injected using a gastight syringe into a Shimadzu QP5050A GC-MS unit through an XTI-F capillary column (150 °C).

Dynamic Light Scattering (DLS)

DLS was performed using a quasi-elastic light scattering spectrometer (Brookhaven 90 Plus Particle Size Analyzer) under 678 nm wavelength laser irradiation. MWNT samples before and after 60 days of the enzymatic degradation were dispersed in 3 mL double-distilled water by sonication for 2 hr forming a translucent suspension, and DLS data were taken by averaging results from 5 runs with each run lasting for 1 min.

Results and Discussion

Carboxylation of MWNTs through acid treatment

It was previously shown that the exposure of either SWNTs or MWNTs to oxidative conditions (such as concentrated oxidative acids) could cause shortening in the length and introduction of defects on both the ends and side walls of carbon nanotubes.[11,34,35] The defects are functionalized by oxygen-containing groups including mainly carboxylic groups, but also lactonic and phenolic groups.[36] In this experiment, MWNTs were first purified with nitric acid pretreatment, after that, there was almost no catalytic iron content left in the sample as shown by thermogravimetric analysis (TGA) and elemental analysis (Supporting Information (SI), Figure S1). Then MWNTs were carboxylated by sonication in H_2SO_4/HNO_3 mixture for 5 hr and 8 hr respectively.

Figure 1 shows the Raman spectra of pretreated, 5 hr, and 8 hr carboxylated MWNTs before the enzymatic degradation process. The spectra were normalized to the G band at around 1570 cm^{-1} in order to compare the change in the D band at around 1323 cm^{-1}. The D to G band intensity ratio was observed to be increasing proportionally to carboxylation time. Since the D band characterizes the disorder-induced mode due to symmetry-lowering effects such as defects in sp^2 hybridized carbon systems,[37,38] the increase in D to G band intensity suggests an increase of defect sites introduced on MWNTs. In order to quantify the functional group loadings on CNTs' surfaces, we performed an acid–base titration[39] following a modified procedure.[36,40] As expected, the titration results showed an increasing acidic group loading along with increasing carboxylation time (SI, Figure S2), indicating that the surface functional group loadings are positively correlated with the amount of defect sites on MWNTs as quantified by TGA (SI, Figure S3). It should be mentioned that it is possible that small amounts of defects were also introduced on p-MWNTs' surface during the pretreatment process. Fourier transform infrared spectroscopy (FTIR) further revealed the existence of oxygen-containing functionalities on MWNT samples (SI, Figure S4).

Enzymatic degradation of carboxylated MWNTs

Our previous study suggested that oxygen-functionalized defects play an important role in facilitating the enzymatic degradation process of SWNTs by providing hydrophilic binding sites for HRP molecules.[29] Since MWNTs are essentially multiple layers of concentric SWNTs, similar degradation behaviors on carboxylated MWNTs were expected. To compare the degradation kinetics of differently carboxylated MWNTs, samples of p-MWNT, o-MWNT (5hr) and o-MWNT (8hr) were investigated. MWNTs were first incubated with HRP for 24 hr to allow sufficient interaction between the enzyme and the substrate, and the reaction was initiated by adding 8 mL of 800 μM H_2O_2 into the suspension. In comparison to our previous work,[28,29] 800 μM H_2O_2 (as opposed to 80 μM) was used in the presence of HRP. We speculated that by raising H_2O_2 concentration an order of magnitude, the degradation kinetics would be greatly accelerated, without denaturing HRP.[29] Upon daily additions of 250 μL H_2O_2 for over 60 days, visual evidence of degradation was observed as shown in Figure 2. The photographs of sample vials taken on Day 0 (Figure 2a) and Day 60 (Figure 2b) show an apparent decrease in light scattering and absorbance from the solutions of o-MWNT (5hr) and o-MWNT (8hr). This observation might indicate a decrease in MWNT concentration after the degradation process, and it appeared that the p-MWNT samples were less degraded compared to the others.

To confirm this observation, Dynamic Light Scattering (DLS) measurements were implemented for all three samples before and after degradation (Figure 2c). It should be noted that DLS calculates the effective hydrodynamic radii of the particles which are

presumably considered as spherical and monodisperse, thus the DLS data do not reflect the actual sizes of MWNTs. The data showed a significant decrease in size distribution after 60 days of degradation process. This decrease could be attributed to two effects: a decrease in the actual sizes (i.e. diameters and lengths) and (or) a decrease in the bundling effect of carbon nanotubes. While the bundling effect is primarily due to the π-π interaction between the sidewalls of nanotubes,41 a decreased bundling effect could point to disturbance in the surface sp^2 carbon system. Thus for both reasons, the DLS data suggested the fact that MWNTs were being degraded. It is seen that the pretreated MWNTs were also degraded, albeit to a lesser degree; this was possibly because of the small amount of defects introduced on to the nanotubes during the pretreatment process.

Transmission electron microscopy (TEM) was used to track the morphological changes of MWNTs as a result of enzymatic degradation (Figure 3). Before incubation with HRP and H_2O_2 (Day 0), all the carbon nanotube samples appeared to be intact with lengths of approximately 1 μm. After 4 days of incubation, it was seen that the boundary of nanotubes began to be distorted, forming carbonaceous sheets that spread among nanotubes. This phenomenon became more significant as the carboxylation time increased. For o-MWNT (8hr) samples, the carbonaceous sheets became prevalent in the visual field surrounding most of the tubular structures. After 30 days, the continuous sheet structures were broken down into nebulous “flakes”. For the 8 hr carboxylated samples, most of the tubular structures became more undefined, and there appeared to be holes forming on these carbonaceous materials. The nanotubes and the residual flakes continued to undergo degradation in following days. At Day 60, it was shown that the sizes of both nanotubes and flakes significantly decreased for o-MWNT (5hr) and o-MWNT (8hr) samples. The length of 8 hr carboxylated MWNTs was shortened from an initial 1 μm to around 100 – 400 nm, and significant bundling effects were not seen over 60 days as each nanotube was surrounded by a layer of carbonaceous sheets. The TEM images showed that MWNT samples with a higher degree of carboxylation have a faster degradation rate. It was observed that the pretreated MWNTs were also undergoing a degradation process, but at a much slower rate. The degradation experiment was continued for another 20 days (Day 80). From TEM images (SI, Figure S5) it was seen that there were no apparent changes to remaining nanotubes, while the carbonaceous flakes (SI, Figure S6) oxidized into progressively smaller pieces. This observation suggested that the degradation of nanotubes was inhibited in the later stage of degradation. It should be mentioned that the decrease in degradation rate is not because of denaturing of the HRP enzyme, because after the degradation process, an Amplex Red assay29 was carried out for each sample and showed no decrease in the enzymatic activity (SI, Figure S7).

Since the degradation process is a further oxidation of carboxylated nanotubes, a final degradation product of carbon dioxide (CO_2) is expected. The CO_2 content in the headspace was monitored by GC-MS. Figure 4 shows the CO_2 (m/z: 44) content relative to N_2 (m/z: 28) in the headspace measured at Days 0, 9 and 35 of incubation. Compared to the control sample (HRP and H_2O_2, no CNTs), CO_2 was evolved progressively for all three MWNT samples. The CO_2 concentration increased 4 – 5 times the initial level at Day 35 for MWNT samples while remaining relatively stable for the control. Furthermore, the trend that more carboxylated MWNTs had a faster CO_2 evolution was observed as expected.

In addition, Raman spectroscopy (Figure 5) was performed to characterize the degradation process. It is known that the tangential G band and disorder-induced D band are characteristic for graphitic carbon materials,42 thus their intensities can reflect the abundance of graphitic material present in degraded samples. The Raman samples were prepared by drop-casting and drying the residual suspension on quartz slide in ambient (SI, Figure S8). All Raman spectra were baseline-corrected in order to compare the D and G

band changes. For o-MWNT (5hr) and o-MWNT (8hr) samples, the intensities of both D and G bands were seen to decrease progressively, suggesting a gradual diminishing of graphitic material so that only a small portion was left in the sample after 60 days of degradation. For p-MWNT samples, however, the G band intensity remained the same at Day 30 to Day 60, while D band intensity continued to decrease as the enzymatic degradation progressed. The decrease in D to G band intensity ratio (I_D/I_G) was also observed in o-MWNT (5hr) and o-MWNT (8hr) samples (Figure 5). It should be reminded here that in the case of SWNT enzymatic degradation,30 the D to G band ratio increased monotonically until both bands were completely suppressed, indicating an increasing defective site abundance created during degradation. However, for p-MWNT and o-MWNT (5hr) samples, it was seen that the D to G band ratio increases during the first 30 days of incubation, but decreases in the next 30 days. Such an observation alludes to a more complex degradation mechanism for MWNTs (Scheme 1).

Unlike SWNTs, MWNTs have multiple graphitic layers. During the carboxylation process, the oxidative acid can create defects within the first several layers of sidewalls12 and also to both ends.10 These defects (oxygen functionalities) presumably provide preferable binding sites for the enzyme,29 thus the degradation will start from both ends as well as the defective sites on the outer layers of sidewalls. When the outer layers undergo enzymatic degradation, the graphitic structures are further oxidized and thus the D to G band ratio increases. However, following this further oxidation, the graphitic lattice becomes more distorted and is exfoliated from the nanotubes, forming carbonaceous residues which presumably do not have characteristic Raman bands. Thus, as the outer layers are peeled off, further Raman spectra were essentially collected on exposed inner layers. It may be that oxidative acids cannot effectively oxidize the inner layers, which would result in their more pristine structure compared to outer layers. Therefore, the D to G band ratio would decrease when the outer graphitic layers were degraded and the inner layers were exposed. In this sense, the degradation rate of all three samples would greatly slow as pristine inner layers are more resistant to enzymatic degradation. Comparing the D to G band ratios for all three samples at Day 60, we found that p-MWNTs were the most pristine (with little influence from inner wall oxidation). This may be why the pretreated sample had the slowest degradation kinetics. Conversely, the degradation rate of o-MWNT (8hr) was comparatively accelerated, showing an effect that degradation may have penetrated through additional walls, as the D to G band ratios progressively decreased during 60 days.

While the enzymatic degradation from both ends of MWNTs would shorten the nanotube length, as clearly shown in TEM images, the degradation from the sidewalls would cause decrease in the nanotube diameters. To verify the degradation mechanism, the diameter distributions of MWNT samples were measured from low-resolution TEM images. For each sample before and after 60 days of degradation, 100 measurements of nanotube diameters were obtained and shown in Figure 6, with the corresponding average values listed above. Nanotube diameters from all three samples significantly decreased after 60 days of incubation from approximately 14 nm to 8 – 11 nm. This diameter decline can only be attributed to the fact that the outer layers of MWNTs were etched away by the enzyme. Since the interlayer spacing of MWNTs was reported to approach 0.344 nm when the diameters are over 7 nm,43 the statistical data can roughly tell the number of layers that have been oxidized. Based on the assumption of 0.688 nm in diameter reduction per layer oxidized, on average, there were approximately 3 layers degraded for the p-MWNT samples, and 7 to 8 layers for o-MWNT (5hr) and o-MWNT (8hr) samples.

To better reveal structural morphology, high-resolution TEM imaging was performed on o-MWNT (8hr) samples before and after 60 days of degradation (Figure 7a, b). The initial MWNTs were observed with diameters around 16 nm and 13 – 14 graphitic walls; while the

diameters of degraded MWNTs reduced to around 8 nm with 5 – 6 graphitic walls. The high-resolution TEM (SI, Figure S9a) also shows that there are defective sites on o-MWNT (8hr) samples where the lattice structures within 5 – 8 outer graphitic layers were broken by the effect of oxidative acids.

Enzymatic degradation of nitrogen-doped MWNTs

The post-synthesis functionalization methods such as carboxylation with strong oxidizing agents can introduce defective sites only in outer walls, which retain the pristine inner layers that are resistant to enzymatic degradation. However, MWNTs can also be intrinsically functionalized by doping with nitrogen atoms during the synthesis process. By introduction of nitrogen source (MeCN) into the liquid precursor, the CVD synthesis produces a tubular structure compartmented by stacked cup-shaped sections as a result of nitrogen doping. Previous research16,44 showed that the graphitic walls between two adjacent cups are not connected but extend outward unparallel to the tubular axis. As nitrogen has one more electron than carbon, the doped nitrogen atoms are not compatible to the graphitic structure and energetically prefer to stay at the open edge of the discontinuous graphitic walls forming dangling bonds.45 In this case, there are nitrogen-functionalized defective sites throughout all graphitic walls in n-MWNTs.

Figure 8a shows an n-MWNT after purification process. Unlike MWNTs with continuous and hollow tubular structures, the nitrogen doping causes compartmentalization in the nanotube forming small stacked cups about 40 nm in length. For enzymatic degradation, the n-MWNT samples were incubated under the same HRP conditions as o-MWNTs with daily addition of 800 μM H_2O_2. TEM images tracked the morphological changes of n-MWNTs. On Day 15 (Figure 8b), the distinctive edge of the nanotubes became unidentified; the tubular structure started to be distorted, and there appeared to be carbonaceous sheets surrounding each nanotube. These results were consistent to the observations of o-MWNTs at the initial stage of degradation. After 50 days (Figure 8c), these carbonaceous sheets were observed to spread all over the sample, with holes appearing on top of them, which indicated further degradation of the carbonaceous sheets. However, the tubular structure was hardly observed at this stage, and they appeared to be merging into the sheets. Eventually, at Day 80, there were no tubular structures observed, and the only materials left over were some amorphous flakes. The absence of tubular structures showed a complete degradation behavior of n-MWNTs by HRP/H_2O_2. Photograph images (Figure 8e) taken before and after 90 days of degradation process showed a significant disappearance of the grey color in the solution. This complete degradation of n-MWNTs was further confirmed by Raman spectroscopy (Figure 8f), which shows almost complete absence of D and G bands after enzymatic degradation.

This observation showed a significant contrast to the incomplete enzymatic degradation of o-MWNTs, further supporting the “layer-by-layer” degradation mechanism proposed above. In essence, the nitrogen doping introduces much more defects into the graphitic structure, which can be reflected from the Raman spectra (Figure 8f) because the D/G band ratio of n-MWNTs are much higher than that of o-MWNTs. Since nitrogen was doped *in situ* during the synthesis process, these defective sites not only exist in the outer graphitic layers, but are present in all graphitic walls. These nitrogen functionalized defects are then assumed to provide binding sites for HRP enzyme throughout the whole process leading to complete degradation.

It should be noted here that the as-synthesized n-MWNTs were subject to a purification process with HCl and H_2O_2 in order to reduce the content of iron impurities. Thermogravimetric analysis (TGA) taken on the samples before and after purification showed that there was a considerable decrease in the iron content after purification, although

the left-over iron content was still significant (SI, Figure S10a). It is possible that the residual iron impurities may cause a Fenton catalytic oxidation29 of n-MWNTs and influence the result of enzymatic degradation. In a control experiment, we replaced the HRP by 1×10^{-4} M $FeCl_3$ aqueous solution with daily addition of the same amount of H_2O_2, in order to study Fenton oxidation of n-MWNTs. However, after 80 days of incubation, there were still a considerable amount of nanotubes were observed in TEM images (SI, Figure S10b), which showed that the Fenton oxidation may have much slower degradation kinetics on n-MWNTs than HRP/H_2O_2. Thus, the effect of iron impurities on HRP/H_2O_2 enzymatic degradation was minor.

Conclusion

In this study, the enzymatic degradation of carboxylated MWNTs and nitrogen-doped MWNTs was investigated in the presence of HRP and H_2O_2. Different degrees of carboxylation were achieved by controlling the time of oxidative acid treatment, and the resultant degradation rate was associated with the degree of carboxylation on MWNTs, which further supported the fact that it is the hydrophilic interaction between HRP's heme active site and the oxygen-containing defective sites on nanotubes that causes the nanotubes to be oxidized and degraded, as we concluded in our previous work.29 The degradation was confirmed by monitoring the evolution of CO_2 gas as a final oxidation product by GC-MS. Furthermore, because of their multi-layer graphitic structures, the MWNTs are more resistant to HRP degradation and it takes a significantly longer time to degrade MWNTs than SWNTs in the same experimental conditions. The fact that MWNTs with reduced diameters and lengths remained over 80 days of degradation leads to a layer-by-layer mechanism of degradation revealed by TEM and Raman spectroscopy. The degradation of MWNTs is taking place on the defective sites of outer graphitic walls which are exfoliated layer-by-layer leaving the pristine inner walls more resistant to HRP oxidation. In contrast to carboxylated MWNTs, nitrogen-doped MWNTs, having intrinsic nitrogen-functionalized defective sites in all graphitic walls, showed complete enzymatic degradation within 80 days, which well supported the proposed mechanism.

Supplementary Material

Refer to Web version on PubMed Central for supplementary material.

Acknowledgments

The project described was supported by Award Number R01ES019304 form the National Institute of Environmental Health Sciences. The content is solely the responsibility of the authors and does not necessarily represent the official views of the National Institute of Environmental Health Sciences or the National Institutes of Health. The authors thank Tom Harper and NFCF for the provision of access to the instruments.

REFERENCES

1. Iijma S. Nature. 1991; 354:56–58.
2. Baughman RH, Zakhidov AA, de Heer WA. Science. 2002; 297:787–792. [PubMed: 12161643]
3. Odom TW, Huang J-L, Kim P, Lieber CM. J. Phys. Chem. B. 2000; 104:2794–2809.
4. Tasis D, Tagmatarchis N, Bianco A, Prato M. Chem. Rev. 2006; 106:1105–1136. [PubMed: 16522018]
5. Hwang GL, Hwang KC. J. Mater. Chem. 2001; 11:1722–1725.
6. Blake R, Gun'ko YK, Coleman J, Cadek M, Fonseca A, Nagy JB, Blau WJ. J. Am. Chem. Soc. 2004; 126:10226–10227. [PubMed: 15315418]
7. Kauffman DR, Star A. Angew. Chem., Int. Ed. 2008; 47:6550–6570.
8. Allen BL, Kichambare PD, Star A. Adv. Mater. 2007; 19:1439–1451.

9. Kauffman DR, Shade CM, Uh H, Petoud S, Star A. Nat. Chem. 2009; 1:500–506. [PubMed: 21378918]
10. Chen J, Chen S, Zhao X, Kuznetsova LV, Wong SS, Ojima IJ. Am. Chem. Soc. 2008; 130:16778–16785.
11. Wu W, Wieckowski S, Pastorin G, Benincasa M, Klumpp C, Briand J-P, Gennaro R, Prato M, Bianco A. Angew. Chem., Int. Ed. 2005; 44:6358–6362.
12. Osswald S, Havel M, Gogotsi Y. J. Raman Spectrosc. 2007; 38:728–736.
13. Kauffman DR, Tang Y, Kichambare PD, Jackovitz JF, Star A. Energ. Fuels. 2010; 24:1877–1881.
14. Flahaut E, Bacsa R, Peigney A, Laurent C. Chem. Commum. 2003:1442–1443.
15. Rosca ID, Watari F, Uo M, Akasaka T. Carbon. 2005; 43:3124–3131.
16. Allen BL, Kichambare PD, Star A. ACS Nano. 2008; 2:1914–1920. [PubMed: 19206432]
17. Gong K, Du F, Xia Z, Durstock M, Dai L. Science. 2009; 323:760–764. [PubMed: 19197058]
18. Tang Y, Allen BL, Kauffman DR, Star A. J. Am. Chem. Soc. 2009; 131:13200–13201. [PubMed: 19722487]
19. Eklund, P.; Ajayan, P.; Blackmon, R.; Hart, AJ.; Kong, J.; Pradhan, B.; Rao, A.; Rinzler, A. Baltimore, MD: World Technology Evaluation Center, Inc.; 2007. WTEC Panel Report on International Assessment of Research and Development of Carbon Nanotube Manufacturing and Applications. p. 7-17.
20. Hyung H, Fortner JD, Hughes JB, Kim J-H. Environ. Sci. Technol. 2007; 41:179–184. [PubMed: 17265945]
21. Kennedy AJ, Hull MS, Steevens JA, Dontsova KM, Chappell MA, Gunter JC, Weiss CA Jr. Environ. Toxicol. Chem. 2008; 27:1932–1941. [PubMed: 19086318]
22. Jia G, Wang H, Yan L, Wang X, Pei R, Yan T, Zhao Y, Guo X. Environ. Sci. Technol. 2005; 39:1378–1383. [PubMed: 15787380]
23. Poland CA, Duffin R, Kinloch I, Maynard A, Wallace WAH, Seaton A, Stone V, Brown S, MacNee W, Donaldson K. Nat. Nanotechnol. 2008; 3:423–428. [PubMed: 18654567]
24. Singh R, Pantarotto D, McCarthy D, Chaloin O, Hoebeke J, Partidos CD, Briand J-P, Prato M, Bianco A, Kostarelos K. J. Am. Chem. Soc. 2005; 127:4388–4396. [PubMed: 15783221]
25. Kam NWS, Jessop TC, Wender PA, Dai H. J. Am. Chem. Soc. 2004; 126:6850–6851. [PubMed: 15174838]
26. Konduru NV, Tyurina YY, Feng W, Basova LV, Belikova NA, Bayir H, Clark K, Rubin M, Stolz D, Vallhov H, Scheynius A, Witasp E, Fadeel B, Kichambare PD, Star A, Kisin ER, Murray AR, Shvedova AA, Kagan VE. Plos One. 2009; 4:1–17.
27. Liu Z, Davis C, Cai W, He L, Chen X, Dai H. Proc. Natl. Acad. Sci. 2008; 105:1410–1415. [PubMed: 18230737]
28. Allen BL, Kichambare PD, Gou P, Vlasova II, Kapralov AA, Konduru N, Kagan VE, Star A. Nano. Lett. 2008; 8:3899–3903. [PubMed: 18954125]
29. Allen BL, Kotchey GP, Chen Y, Yanamala NVK, Klein-Seetharaman J, Kagan VE, Star A. J. Am. Chem. Soc. 2009; 131:17194–17205. [PubMed: 19891488]
30. Kagan VE, Konduru NV, Feng W, Allen BL, Conroy J, Volkov Y, Vlasova II, Belikova NA, Yanamala N, Kapralov A, Tyurina YY, Shi J, Kisin ER, Murray AR, Franks J, Stolz D, Gou P, Klein-Seetharaman J, Fadeel B, Star A, Shvedova AA. Nat. Nanotechnol. 2010; 5:354–359. [PubMed: 20364135]
31. Russier J, Ménard-Moyon C, Venturelli E, Gravel E, Marcolongo G, Meneghetti M, Doris E, Bianco A. Nanoscale. [Online early access].
32. Wang Y, Shan H, Hauge RH, Pasquali M, Smalley RE. J. Phys. Chem. B. 2007; 111:1249–1252. [PubMed: 17249726]
33. Hunt JP, Taube H. J. Am. Chem. Soc. 1952; 74:5999–6002.
34. Liu J, Rinzler AG, Dai H, Hafner JH, Bradley RK, Boul PJ, Lu A, Iverson T, Shelimov K, Huffman CB, Rodriguez-Macias F, Shon Y-S, Lee TR, Colbert DT, Smalley RE. Science. 1998; 280:1253–1256. [PubMed: 9596576]
35. Mawhinney DB, Naumenko V, Kuznetsova A, Yates JT Jr, Liu J, Smalley RE. Chem. Phys. Lett. 2000; 324:213–216.

36. Hu H, Bhowmik P, Zhao B, Hamon MA, Itkis ME, Haddon RC. Chem. Phys. Lett. 2001; 345:25–28.
37. Dresselhaus MS, Jorio A, Hofmann M, Dresselhaus G, Saito R. Nano. Lett. 2010; 10:751–758. [PubMed: 20085345]
38. Ouyang Y, Cong LM, Chen L, Liu QX, Fang Y. Physica E. 2008; 40:2386–2389.
39. Boehm HP, Diehl E, Heck W, Sappok R. Angew. Chem. Int. Ed. 1964; 3:669–677.
40. Scheibe B, Borowiak-Palen E, Kalenczuk R. J. Mater. Charact. 2010; 61:185–191.
41. Bahr JL, Mickelson ET, Bronikowski MJ, Smalley RE, Tour JM. Chem. Commun. 2001:193–194.
42. Dresselhaus MS, Dresselhaus G, Jorio A, Souza Filho AG, Saito R. Carbon. 2002; 40:2043–2061.
43. Kiang C-H, Endo M, Ajayan PM, Dresselhaus G, Dresselhaus MS. Phys. Rev. Lett. 1998; 81:1869–1872.
44. Wang EG. J. Mater. Res. 2006; 21:2764–2773.
45. Zhao GL, Bagayoko D, Wang EG. Modern Phys. Lett. B. 2003; 17:375–382.

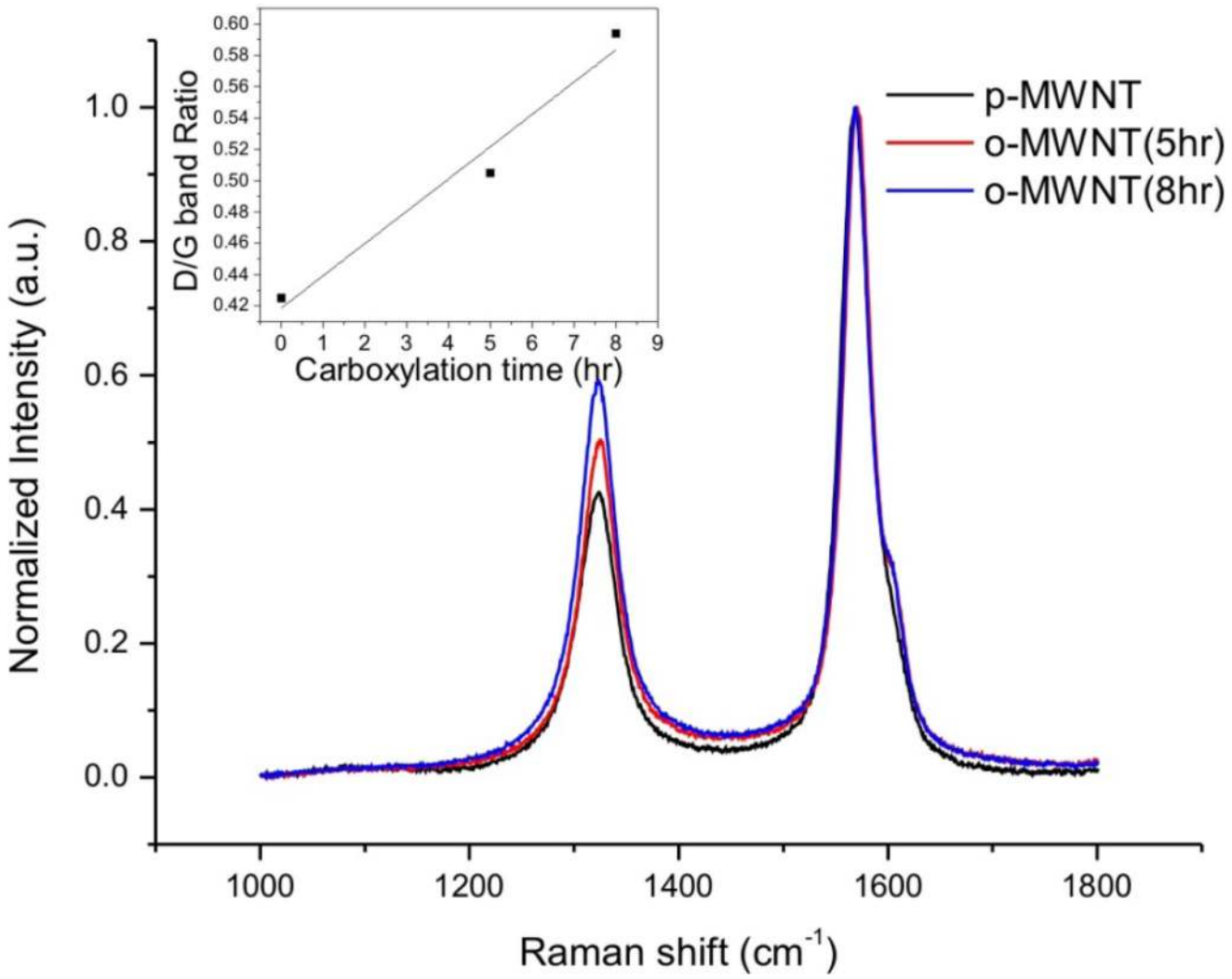

Figure 1.
Normalized Raman spectra of MWNTs with 0 hr (black), 5 hr (red) and 8 hr (blue) carboxylation before degradation. Inset: D to G band ratio vs. carboxylation time.

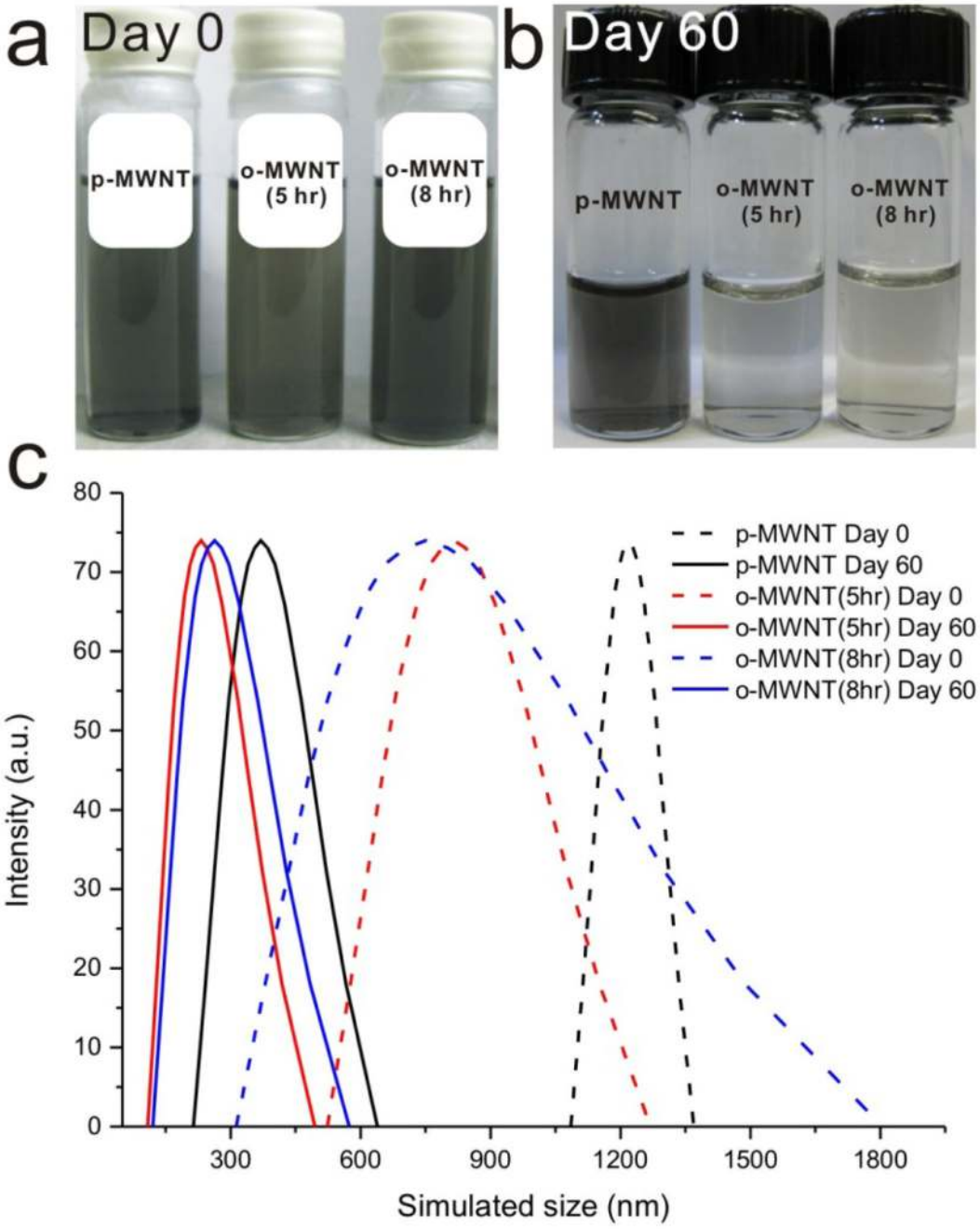

Figure 2.

Photograph showing enzymatic degradation process of MWNTs after carboxylation for different durations on (a) Day 0 and (b) Day 60. (c) Dynamic light scattering (DLS) measurements showing decrease in size distribution of different MWNTs before (dash lines) and after (solid lines) incubation with HRP and H_2O_2 for 60 days.

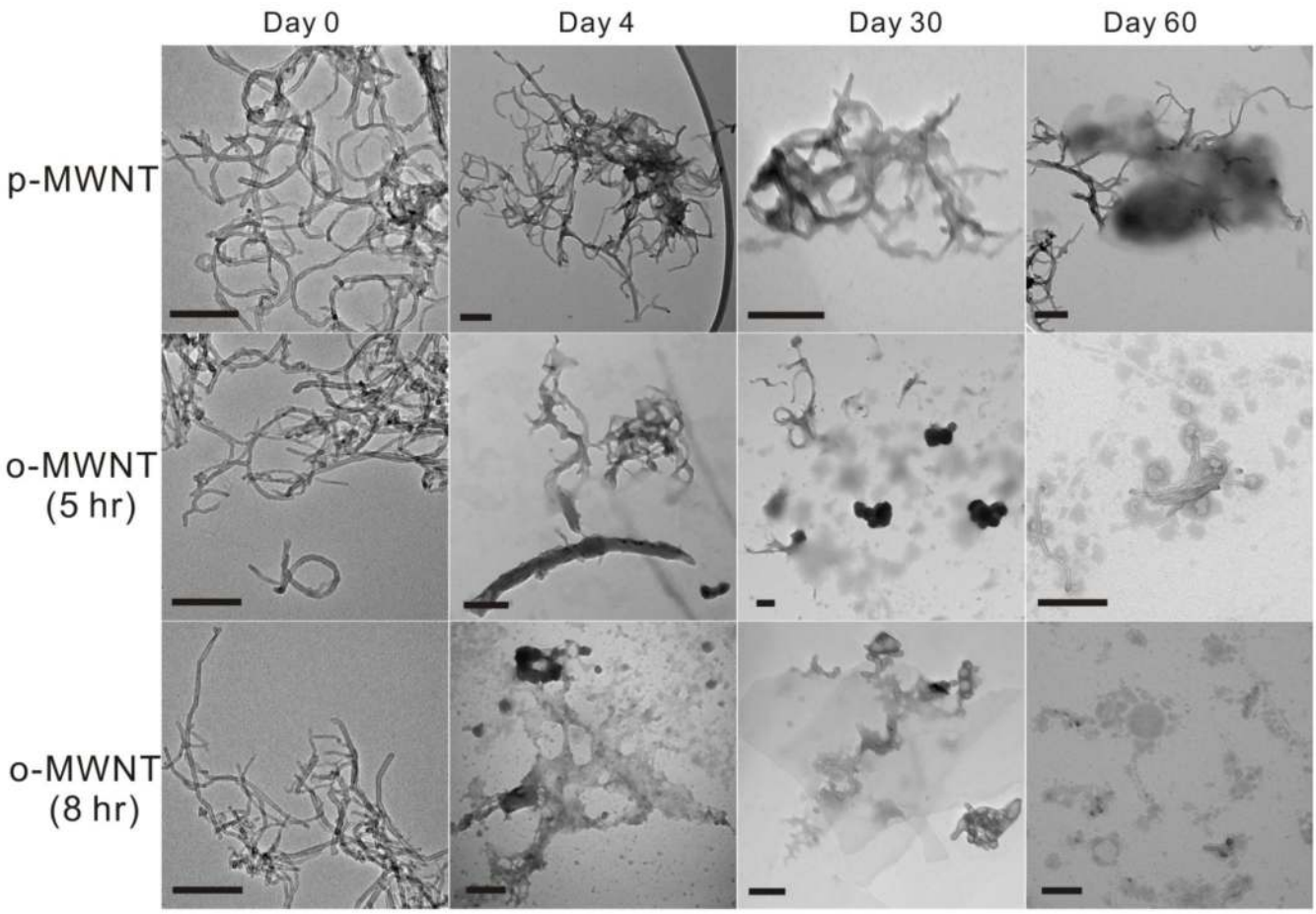

Figure 3.
TEM images of carboxylated MWNTs incubated with HRP and H_2O_2. Each row corresponds to different carboxylation times (0, 5 and 8 hours) and each column corresponds to different enzymatic incubation times (0, 4, 30 and 60 days). All scale bars are 200 nm.

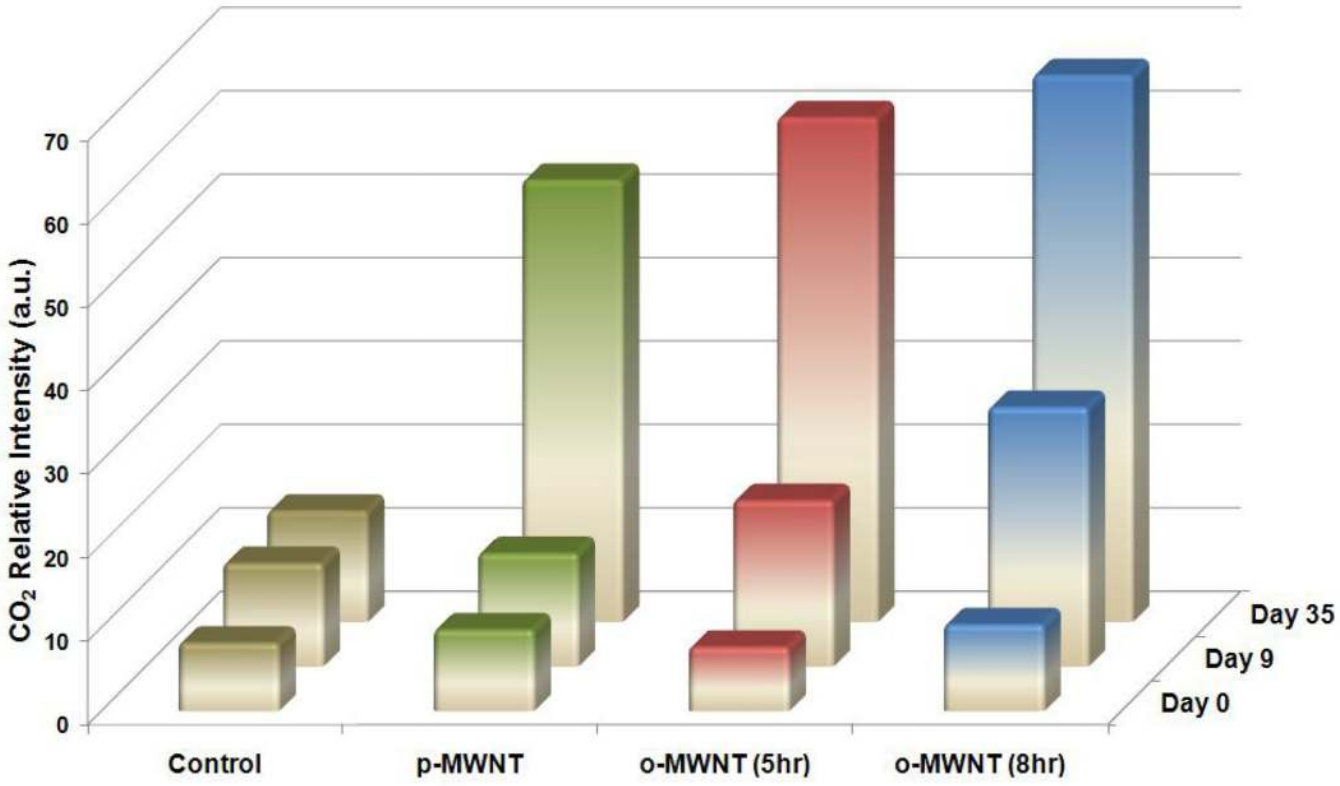

Figure 4.
Evolution of CO_2 in the sample headspace as a final product of MWNT enzymatic degradation measured by GC-MS on Day 0, 9 and 35 of incubating MWNTs with HRP and H_2O_2. The control sample was made by mixing HRP and H_2O_2 only.

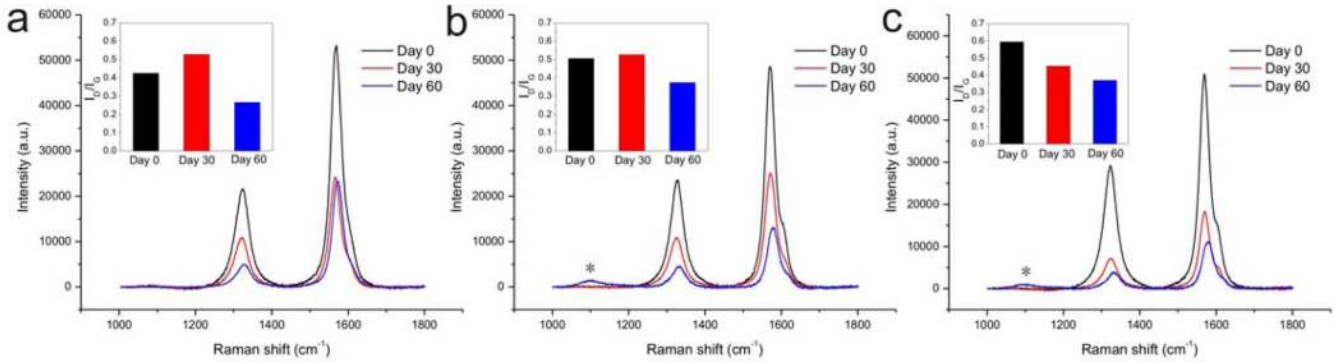

Figure 5.

Raman spectra of (a) p-MWNT, (b) o-MWNT (5hr), and (c) o-MWNT (8hr) showing decay of the D and G band intensity during the enzymatic degradation process (asterisk indicates contribution from quartz substrate). Insets: The changes of D to G band ratio of each sample versus degradation time.

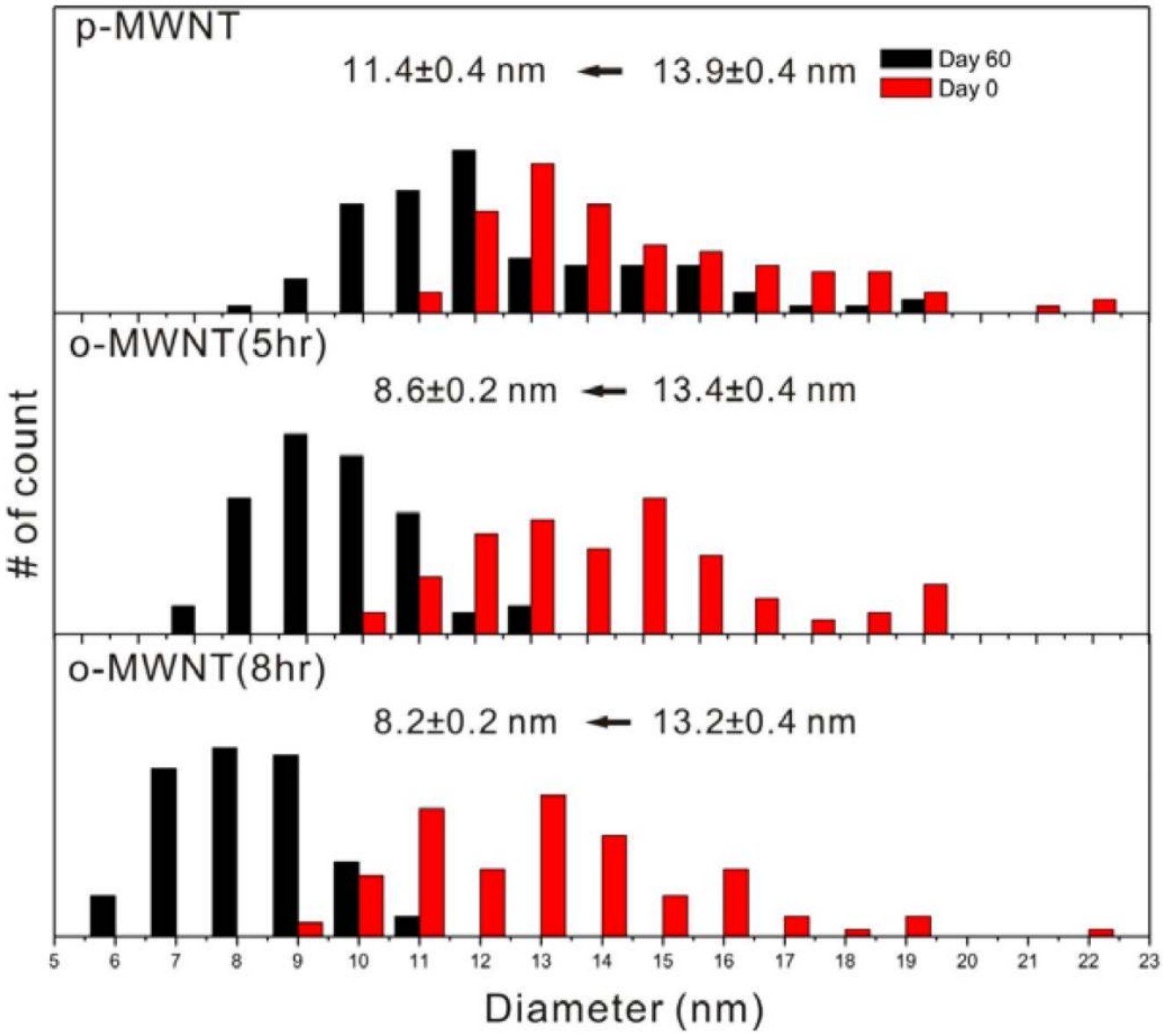

Figure 6.
Comparison of the diameter distributions of MWNTs before and after 60 days of incubation with HRP and H_2O_2. For each sample 100 measurements of nanotube diameters were obtained via TEM imaging. The numbers above each histogram are the corresponding average values.

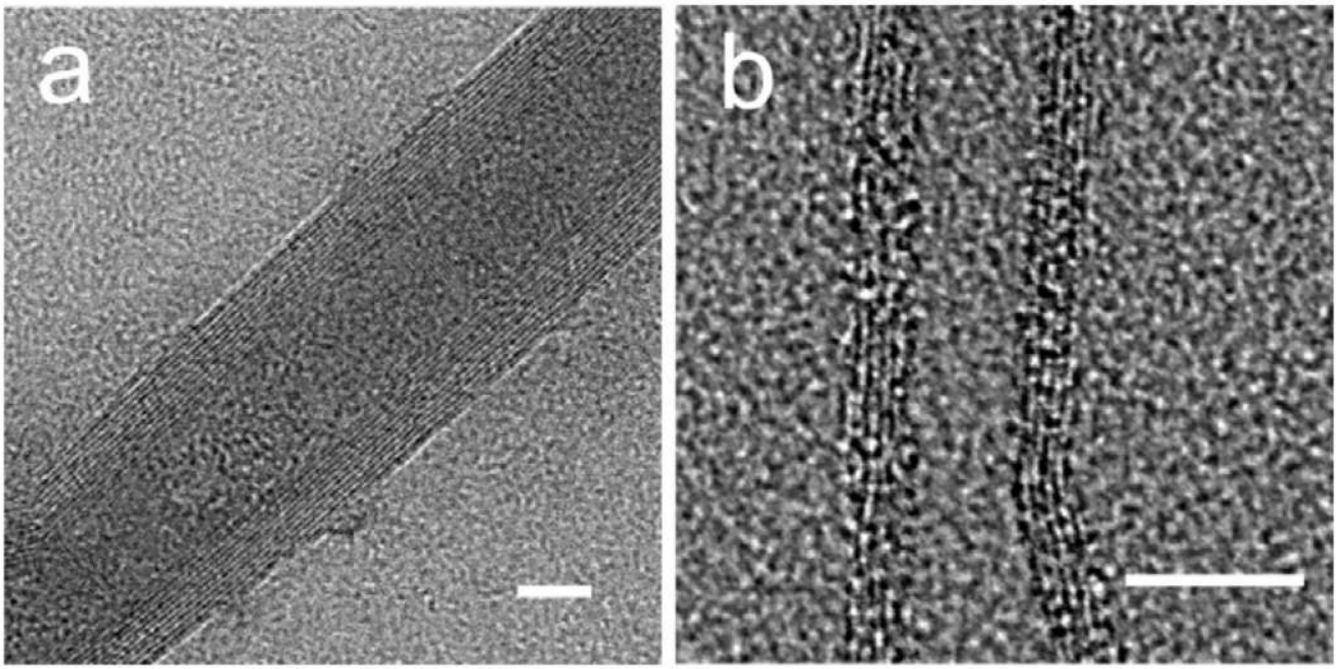

Figure 7.
High-resolution TEM images of o-MWNT (8hr) samples. All scale bars correspond to 5 nm. (a) o-MWNTs (8hr) before enzymatic degradation. (b) o-MWNTs (8hr) after 60 days of enzymatic degradation.

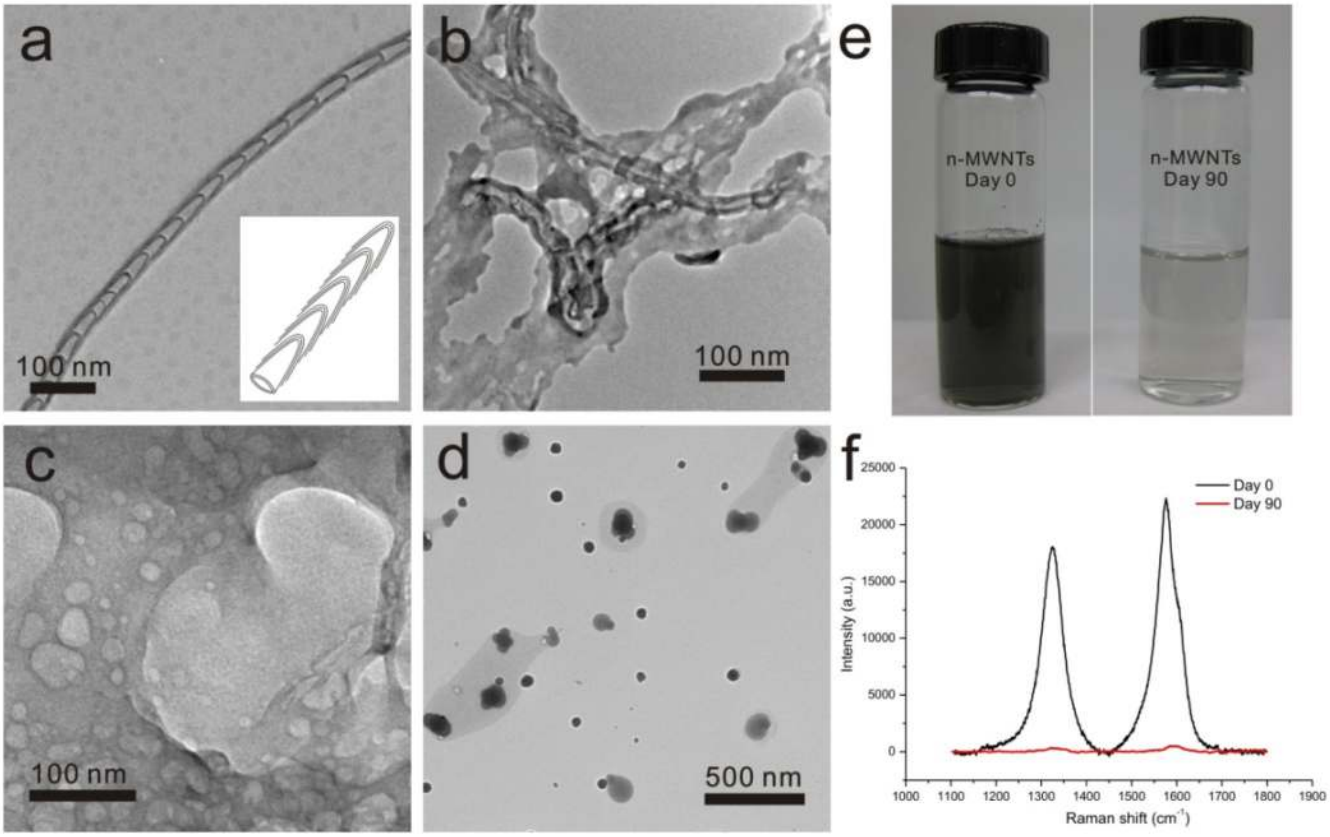

Figure 8.
(a–d) TEM images of nitrogen-doped MWNT (n-MWNT) samples during enzymatic degradation: (a) As synthesized and purified n-MWNT at Day 0. The inset shows the schematic illustration of its stacked-cup structure. (b) Day 15, (c) Day 50, and (d) Day 80. (e) Photographs comparing n-MWNT samples before (left) and after (right) enzymatic degradation. (f) Raman spectra for n-MWNT samples before (black) and after (red) enzymatic degradation.

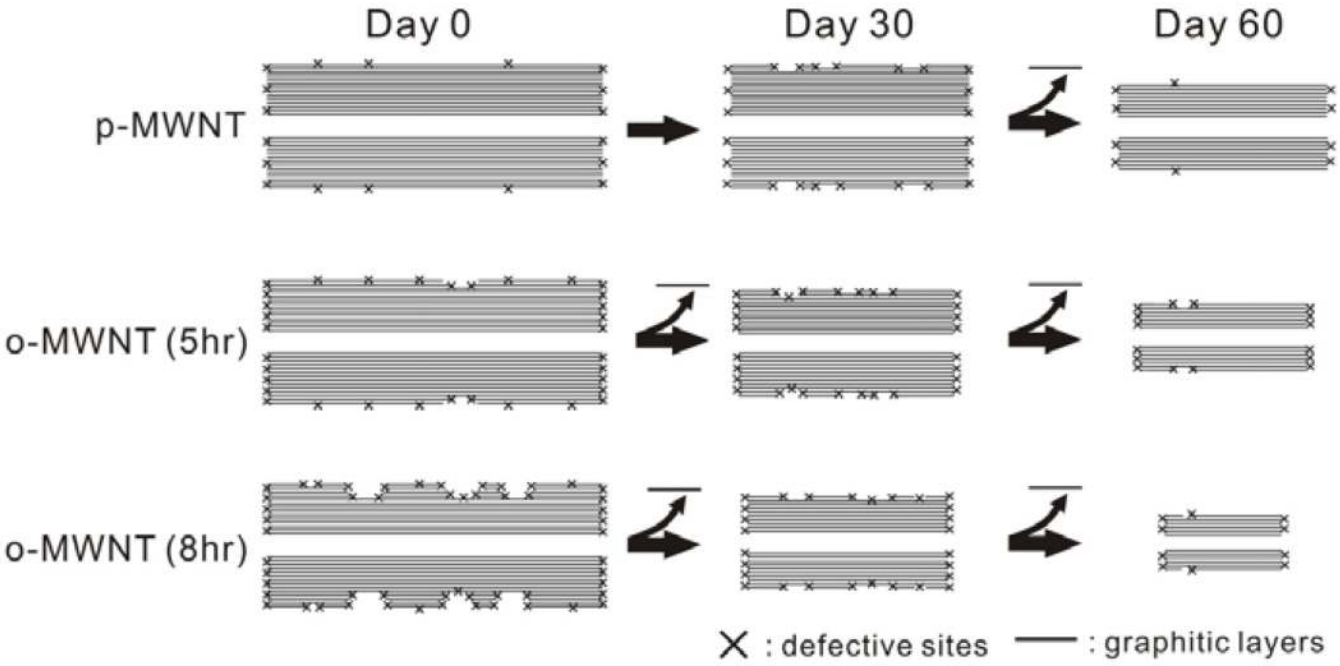

Scheme 1.

Proposed mechanism of MWNT enzymatic degradation. Different carboxylation times result in different amounts of surface defects, which proportionally influence the rate of enzymatic degradation. The degradation of the outer layers produces more defects; while as the outer layers are exfoliated, the more pristine inner core that is resistant to HRP/H_2O_2 degradation is gradually exposed.